Article

pubs.acs.org/Biomac

Molecular Dynamics Simulations of the Adhesion of a Thin Annealed Film of Oleic Acid onto Crystalline Cellulose

Mir A. A. R. Quddus,[†,‡,§] Orlando J. Rojas,[‡,§,⊥] and Melissa A. Pasquinelli*[,‡]

[‡]Fiber and Polymer Science Program and [§]Forest Biomaterials, North Carolina State University, Raleigh, North Carolina 27695, United States

[⊥]School of Chemical Technology, Department of Forest Products Technology, Aalto University, P.O. Box 16300, 00076, Aalto, Finland

ABSTRACT: Molecular dynamics simulations were used to characterize the wetting behavior of crystalline cellulose planes in contact with a thin oily film of oleic acid. Cellulose crystal planes with higher molecular protrusions and increased surface area produced stronger adhesion if compared to other crystal planes due to enhanced wetting and hydrogen bonding. The detailed characteristics of crystal plane features and the contribution of directional hydrogen bonding was investigated. Similarly, oleophilicity of the cellulose planes increased with the increase in surface roughness and number of directional hydrogen bonds. These results correlate with conclusions drawn from experimental studies such as adhesion of an ink vehicle on cellulose surface.

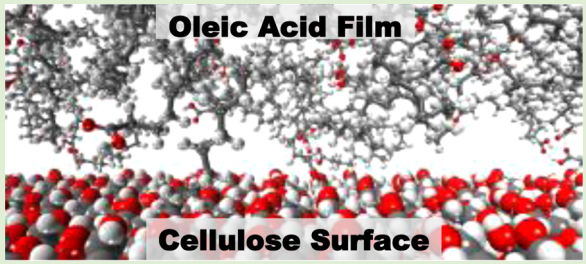

INTRODUCTION

Cellulose is known for its ability to absorb moisture and is one of the most widely used natural polymers in both the textile and paper industries. Formation of a fluid film on cellulose surfaces, for example, from condensing water and oily substances, is an ubiquitous phenomenon; in the latter case, oil surface excess can diminish the capabilities for moisture absorption and affect functional fiber properties, including its susceptibility for processing, cleaning, and laundering. Commonly known sources of oily adsorbates are wood extracts,[1] sebaceous gland secretions,[2] and lubricants[3] that routinely come in contact with cellulosic surfaces during production, conversion, or use. Therefore, an understanding of the interactions between oily substances and cellulose is critical in applications such as self-cleaning,[4−9] waterproofing,[10,11] selective filtering and separation[12−14] packaging,[15] drug delivery,[16,17] and lubrication.[18,19] It could also help in the design of materials with controlled biofilm growth[20] and for the sorption and recovery of oil.[21]

Adhesion between a surface and a fluid requires interfacial molecular contact, which highlights the importance of surface topography and roughness[22,23] and also wetting and spreading of the fluid over the surface. Additionally, chain segments or phase components may undergo diffusion to the interfacial zone, resulting in a minimization of the total free energy of the system. The intimate contact between the fluid and the solid can be achieved by various attractive intermolecular and interatomic forces across the interface.[24−27] In its simplest form, the adhesion can be described by the thermodynamic work of adhesion, which can be calculated from the interfacial free energies. In the case of cellulose, several effects have been examined, such as mechanical interlocking, adsorption or wetting theory, diffusion theory, and the theory of weak boundary layers.[28]

Cellulose is known for its ability to form strong hydrogen bonds with interacting surfaces or molecules due the presence of hydroxyl groups on the surface.[29−31] However, despite the presence of water loving hydroxyl groups, cellulose is insoluble in water. Generally, it is believed that intermolecular hydrogen bonding is responsible for this phenomenon. Recent studies indicate that the insolubility of cellulose might be due to the subtle balance between hydrogen bonding, with van der Waals (vdW), and hydrophobic interactions.[32,33] In addition, previous studies have identified the role of surface roughness of cellulose on the adsorption of water,[34] lipophilic compounds,[35] organics[36] and enzymes.[37] Fatty acids, which are present in oily materials, have the capability to form hydrogen bonds via carboxylic groups.[38−40] For example, a study conducted on oleic acid adsorbing onto rice hulls indicated that hydrogen bonds with moderate to weak strength were formed between the two components.[39]

The goal of this work is to obtain molecular details about the adhesion of thin oleic acid films onto crystalline cellulose planes (as a mimic for a perfectly crystalline surface) and how the adhesion energies are impacted by the chemical composition and molecular structure of the plane. Oleic acid was chosen as a model fatty acid due to its significance in both paper and the textile applications; for example, a study by Hubbe and co-workers indicated that the hydrophobic character of a cellulose surface can overtake its hydrophilicity when treated with fatty

Received: January 20, 2014
Revised: February 27, 2014

dx.doi.org/10.1021/bm500088c | *Biomacromolecules* XXXX, XXX, XXX−XXX

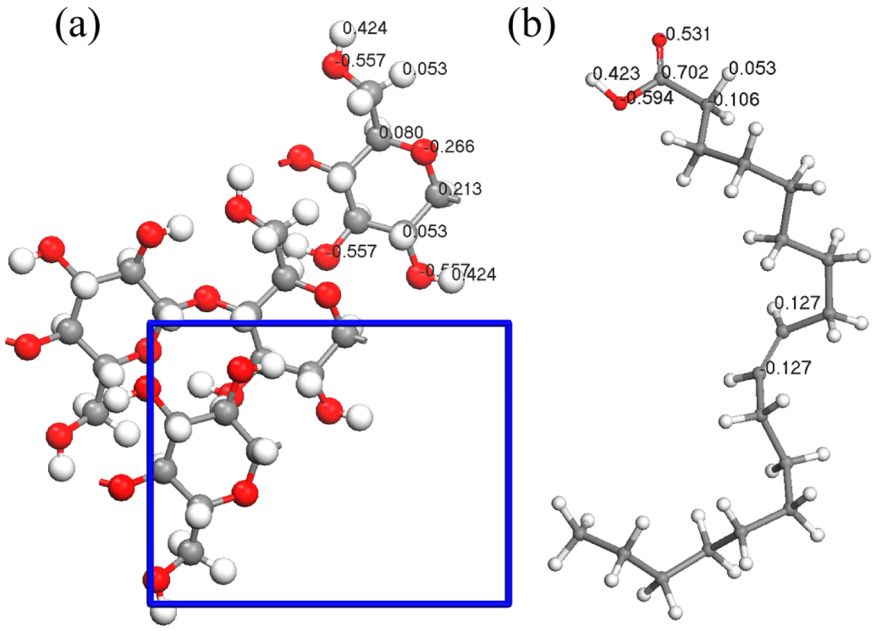

Figure 1. Molecular structure of (a) the cellulose Iβ unit cell,[51] and (b) oleic acid.[50] The partial charges from PCFF for both structures are indicated. The box in (a) indicates cellulose unit cell (cellobiose). Carbon atoms are gray, oxygen atoms are red, and hydrogen atoms are white.

Table 1. Properties of the Crystalline Cellulose Planes that were Used in the MD Simulations[a]

		100	110	010
Miller planes	u	34.3	32.6	32.6
	v	32.6	35.5	32.6
MD box dimensions	x	34.3	32.6	32.6
	y	32.6	35.5	32.6
	z	143.0	142.9	144.9
A_{vdW} (Å^2)		2485	2588	3420
R_m (%)		1.0	1.2	1.6
No. of H-bonds per A_{vdW} ($\times 10^3$)		2.0	2.7	2.9
$E_{pot,nb}$ (kcal/mol)		−3758.6 ± 18.8	−4432.4 ± 18.2	−5463.9 ± 14.0
E_{es} (kcal/mol)		−3387.1 ± 9.9	−4105.9 ± 11.7	−5127.9 ± 11.1
E_{vdW} (kcal/mol)		−371.5 ± 14.1	−326.5 ± 19.6	−336.0 ± 14.7

[a]The energy values are averages over the last 100 ps of the MD simulation trajectory.

acid containing materials such as lignin.[41] This observation also implies that hydrophobic modification of a cellulose surface can render it to be used as an oil absorbent material.

METHODOLOGY

All calculations were performed with Materials Studio suite version 5.5 from Accelrys Inc.[42] A second generation all-atom force field, PCFF, was chosen for this study.[43−47] This force field uses the bond lengths and the bond and torsional angles for calculating the bonded terms. The nonbonded terms are calculated using the 9−6 Lennard-Jones potential for vdW interactions and the Coulombic potential for the electrostatic interactions.

Prepare Molecular Model of System. The cellulose planes used in this study were developed from X-ray diffraction data.[48] A monoclinic Iβ unit cell was prepared from the cellobiose unit cell, which is depicted in Figure 1a. Following the procedure reported by Mazeau and co-workers,[49] the unit cell was subjected to 1 ns of NPT (constant number of atoms, pressure, and temperature) simulation at 1 atm pressure and a temperature of 300 K. The unit cell geometry was further optimized for 5000 cycles with the Forcite Plus module. Each 2D plane was then created by cleaving the optimized unit cell along the [100], [110], and [010] Miller planes, the dimensions of which are given in Table 1. A supercell was created by replicating the 2D plane 3 to 4 times the size of the unit cell the X and Y directions. A 3D cellulose slab was created by replicating the supercell in X, Y, and Z directions, as needed. The final dimensions of the cellulose planes are specified in Table 1. All of the slabs were then equilibrated for another 5000 cycles.

The structure of oleic acid ($C_{18}H_{34}O_2$), given in Figure 1b, was downloaded from the PubChem database.[50] This structure was optimized for 5 ps using the smart algorithm and the PCFF force field. The oleic acid film was prepared by using the Amorphous Builder module. A total of 25 oleic acid molecules were used to prepare this film at the specified oleic acid density of 0.89 g/cm^3.[47] This film was energy minimized for 5000 cycles with Forcite to reduce any energy fluctuations.

To create the entire system, an orthogonal box was generated, and both the oleic acid and the cellulose plane slabs were combined using the Layer Builder utility, where the cellulose plane was put at the bottom of the simulation box. Initially, a distance of 8.5 Å was maintained between the oleic acid film and the plane of the cellulose crystal to avoid steric overlap. A vacuum space of 100 Å was added on top of the oleic acid to restrict its interaction to only the uppermost atom layer of cellulose and also to enhance computational efficiency. The total dimensions of each simulation box are given in Table 1. In addition, apart from the hydroxyl groups located on the topmost section of the cellulose plane, all of the atoms in the bulk cellulose chains were kept constrained by fixing the Cartesian coordinates throughout the minimization and dynamics steps.

dx.doi.org/10.1021/bm500088c | Biomacromolecules XXXX, XXX, XXX−XXX

Simulation Details. All molecular dynamics (MD) simulations were conducted with periodic boundary conditions and explicit treatment of all atoms in the structures. A 9.5 Å cutoff was used for both the electrostatic and vdW terms. All charges applied on the system were based on the atom parameters from the PCFF force field, and are displayed in Figure 1. The minimization was carried out using the conjugate gradient procedure[52] with convergence criteria of a root-mean-square value of less than 0.05 kcal/mol/Å. Unless indicated otherwise, all MD simulations were conducted using the canonical NVT ensemble (constant number of atoms, volume and temperature). The standard Verlet algorithm was applied to iterate the equations of motion in the system. The temperature was controlled with a Nose-Hoover thermostat with a relaxation time of 0.1 ps. A 1 fs time step was used and 300 K temperature was maintained throughout all of the simulations. The simulations were run for a total of 1 ns.

Calculation of System Properties. The cohesive energy density (CED) is the energy that is required to convert a liquid to a gas[53] and can be calculated from the following equation:

$$\mathrm{CED} = \frac{U_v}{M\rho^{-1}} \quad (1)$$

where U_v is the heat of vaporization divided by the molar volume, M is the molar mass, and ρ is the density. The solubility parameter (δ) for the oleic acid film is derived by taking the square root of the CED. It was calculated by first performing a 10 ps geometry optimization followed by 0.5 ps of NVT dynamics, then a temperature cycle from high to low using short NVT and long NPT runs. The density is then equilibrated via NPT, and short NPT production runs are done in order to extract the density.

For the oleic acid film, the temperature at which a second order phase transition (akin to the glass transition temperature in polymers) occurs was determined by subjecting it to NPT simulations. After equilibrating the density using a pressure of 0.1 MPa with a 1 fs time step and the Berendsen barostat, NPT dynamics were performed whereby the temperature was decreased by 25 K every 1000 ps from 350 to 100 K. The average specific volume was calculated at each temperature from four time steps from the production trajectory. When there is a dramatic shift in the trend of specific volume with temperature, the temperature at which that occurs is defined as T_{pt}.[54−56] This temperature is estimated from a plot of specific volume versus temperature by dividing the data into groups based on their linearity, thus, a straight line can be fit through each group and analyzed with linear regression.

The work of adhesion ($W_{adhesion}$) is directly related to the change in interfacial energy due to wetting. It has been used previously to quantify the wettability of thin polymeric films on cellulose,[57] polyester,[58] and other surfaces.[59,60] In general practice, $W_{adhesion}$ is determined from the surface tension values of two interacting surfaces.[61] However, this approach often overestimates $W_{adhesion}$. On the other hand, $W_{adhesion}$ can be calculated by considering the pure physicochemical interaction of the interacting materials.[62] The advantage of this approach is that this model can be varied without the effect of substrate structure, liquid surface tension or viscosity. Thus, $W_{adhesion}$ can be calculated from the following equation:[63,34,57]

$$W_{adhesion} = \frac{E_{inter}}{A_{vdW}} \quad (2)$$

where E_{inter} is the interaction energy between the cellulose and oleic acid film, and A_{vdW} is the vdW contact surface area of the crystalline cellulose plane. The vdW contact surface area was calculated using the Connolly Surface task in Materials Studio by using medium grid resolution, 0.4 Å grid intervals and 2.2 Å Connolly probe radius. The E_{inter} term can be calculated by

$$E_{inter} = E_{total} - (E_{cellulose} + E_{oleic}) \quad (3)$$

where $E_{cellulose}$ and E_{oleic} are the potential energies of cellulose and oleic acid, respectively. A negative value of E_{inter} signifies attraction between the components and a positive value implies repulsion. Thus, a large negative $W_{adhesion}$ value signifies strong adhesion, whereas a smaller negative value (or a positive value) suggests weak adhesion to the plane.

RESULTS AND DISCUSSION

The goal of this work is to investigate the adhesion of a film of oleic acid on three crystalline cellulose planes using MD simulations.

Properties of the Oleic Acid Film. The solubility parameter and T_{pt} were determined previously for each crystalline cellulose plane,[47,64] so we only focus on the oleic acid film here. The solubility parameter of oleic acid is a fundamental property that determines the miscibility of a substance at a given temperature.[65] It is also used to interpret and predict thermodynamic properties of polymer melts and wetting of solid surfaces.[66] At 300 K, the solubility parameter value of 18 $MPa^{0.5}$ was obtained from the simulations for the oleic acid film. This calculated value is close to the experimental value of 15.6 $MPa^{0.5}$ reported by others at the same temperature[55,67] and also to the value calculated via van Krevelen's approximation,[56] which is 17.7 $MPa^{0.5}$. A CED value of 3.2 $MPa^{0.5}$ was obtained from our simulation, which is close to the experimental value[67] of 3.1 $MPa^{0.5}$.

In the plot of the specific volume of the amorphous oleic acid as a function of temperature in Figure 2, a distinct transition

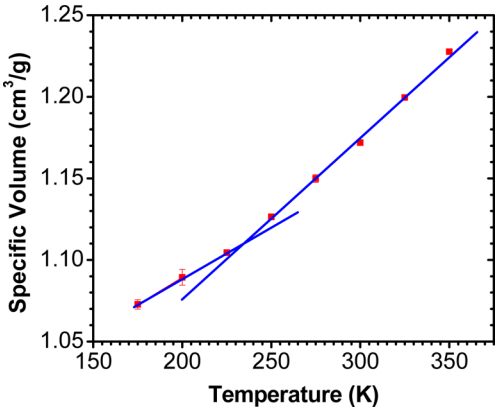

Figure 2. Plot of the specific volume versus temperature for an amorphous oleic acid film at constant pressure of 1 atm. The error bars indicate the standard deviation over 4 different time steps.

was observed to occur around 225 K, which is due to the changes in the specific volume with the reduction in backbone torsion during a phase change. From this plot, T_{pt} was calculated by fitting a linear function through temperatures of 175 to 225 K, and through temperatures of 225 to 350 K, yielding T_{pt} = 225 K. This T_{pt} is very close to the experimentally observed value of 221.3 K for 99.9% pure liquid oleic acid (bulk).[68]

Note that the strong correlation between these calculated quantities and the experimentally determined values validates the use of PCFF for oleic acid; note that this force field has already been validated previously for cellulose.[47,64]

Characterization of the Surface Properties of Crystalline Cellulose. The surface properties of crystalline cellulose were studied previously,[46] but are briefly summarized in Table 1. These values indicate that the [010] plane possesses the highest contact surface area and molecular surface roughness followed by [110] and [100], which is virtually flat. In addition, the [010] plane has one and half times the amount of potential

dx.doi.org/10.1021/bm500088c | Biomacromolecules XXXX, XXX, XXX−XXX

hydrogen bonding sites on the surface than [100]. We also observed in our previous work that the [010] plane has a groove that is wide and deep enough for molecules to penetrate.

Characterization of the System Interface. The total potential energies of the system as a function of time are given in Figure 3 and indicate that the potential energy of all three

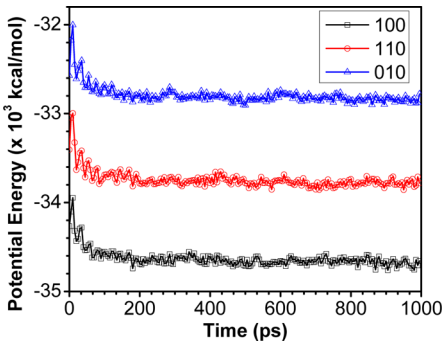

Figure 3. Potential energies of the three systems as a function of time.

systems have equilibrated within the simulation time. The final potential energy of each equilibrated system varied according the following order: [100] > [110] > [010]. The nonbonded contributions to the potential energy in Table 1 indicate that both the vdW and electrostatics have significant contributions in all three systems. As expected, due to the increase in the number of hydroxyl groups on the surface and thus potential hydrogen bonds, the electrostatic contribution is greatest for [010] followed by [110] and then [100]. However, the [100] plane has a slightly higher vdW energy compared to both the [010] and [110] planes. These quantities suggest that the [010] and [110] planes would be more likely to react to the polar oleic acid molecules than the [100] plane.

Figure 4 provides snapshots from final time step of the MD simulation trajectory, and several observations can be made from these equilibrated molecular models. First, in all three systems, the oleic acid film remained intact. In addition, compared to the [110] and [100] planes, the oleic acid molecules can penetrate into the wider and deeper grooves of the [010] planes. These images also display how oleic acid film adhesion and subsequent stability is related to hydrogen bond formation (green dashed lines) at the interface. As indicated in Table 1, the [010] plane has almost twice the number of hydrogen bonding sites per area than the other two planes due to the presence of the deeper grooves, and the [010] plane is observed in Figure 4 to form more hydrogen bonds as compared to the [110] and [100] planes, including those within the grooves.

In order to quantify the number of hydrogen bonds that were formed during the MD simulation, the count of hydrogen bonds formed between oleic acid and each crystalline cellulose plane was calculated using a donor−acceptor distance of 2.5 Å and maximum donor−acceptor angle of 90°. These values are given as a function of simulation time in Figure 5. Overall, the

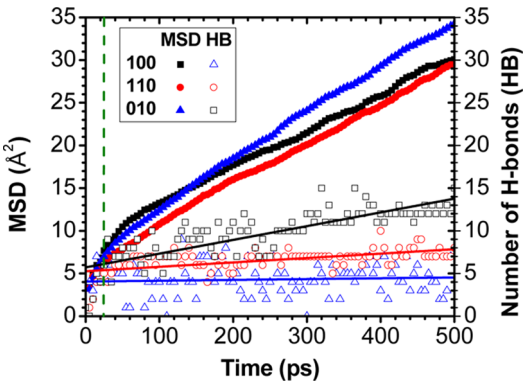

Figure 5. Left axis and solid symbols: Mean squared displacement (MSD) of the carboxyl oxygen of the oleic acid molecules relative to the perpendicular direction of each of the three crystalline cellulose planes; the green dashed line indicates reduction of oxygen atom mobility. Right axis and hollow symbols are the number of hydrogen bonds between oleic acid and each crystalline cellulose plane. The straight lines represent linear fit of the raw data done through regression analysis.

greatest number of hydrogen bonds were formed with the [010] plane, which has the highest molecular surface roughness and overall contact area and, thus, more accessible hydroxyl groups, as indicated in Table 1. The number of hydrogen bonds is observed to increase with simulation time for the [010] plane until about 400 ps, after which it levels off. However, in the case of the [110] and [100] planes, an increase in hydrogen bonding is observed when the oleic acid molecules initially came in contact with the planes (around 20 ps) and then leveled off quickly. Although the [110] cellulose plane has some shallow grooves on its surface (Table 1), there is very little distinction in hydrogen bonding between the [110] and [100] planes. This observation indicates that the grooves are too shallow and narrow to expose additional hydroxyl groups that are accessible to the oleic acid molecules, as suggested by the number of hydrogen bonding sites per area in Table 1.

Another important characteristic of the liquid oleic acid molecules adsorbing on each of the crystalline cellulose planes is the degree of their diffusivity, which can be quantified from

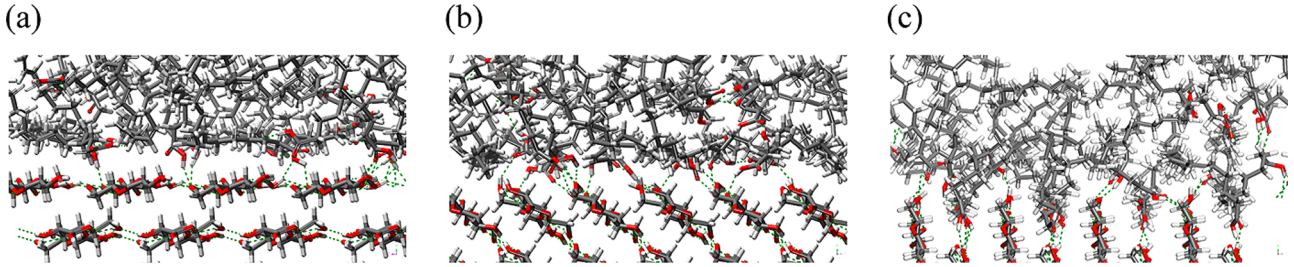

Figure 4. MD snapshots from the 1 ns time step of the oleic acid films on each crystalline cellulose plane: (a) [100], (b) [110], and (c) [010]. Hydrogen bonds are indicated by green dashed lines and the atom color scheme is the same as in Figure 1.

dx.doi.org/10.1021/bm500088c | Biomacromolecules XXXX, XXX, XXX−XXX

the temporal evolution of the mean squared displacement (MSD) from the MD simulation trajectory. Figure 5 provides the temporal evolution of the MSD of the oxygen atoms in the oleic acid molecules, which was calculated perpendicular to each plane. The number of hydrogen bonds between OA and each cellulose plane is also given in Figure 5. The MSD results indicate that the oxygen atoms within the OA film have greater mobility toward the [010] plane than the [110] and [100] planes. It is, however, interesting to note that the initial mobility of the oxygen atoms in oleic acid slowed down due to the formation of hydrogen bonds with the cellulose as the molecules approached each plane. Although the number of hydrogen bonds relatively stabilizes with time, the oleic acid molecules remained relatively mobile, as expected since they are in the liquid phase at this temperature (298 K). Similar observations were made previously, such as for glycerol slowing down toward a carbohydrate (trehalose) due to an increase in intermolecular hydrogen bonding.[69]

The work of adhesion ($W_{adhesion}$) of the oleic acid film interacting with each of the three crystalline planes of cellulose as a function of time is given in Figure 6. The negative values

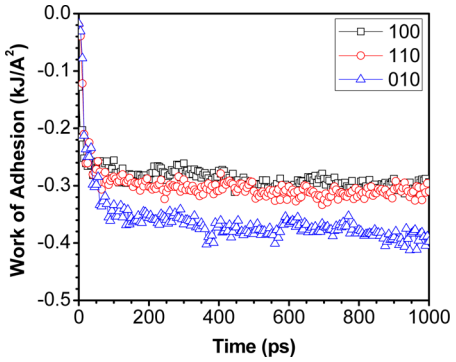

Figure 6. Work of adhesion ($W_{adhesion}$) of the three crystalline cellulose planes covered with an amorphous film of oleic acid. The Connolly surface area was used in the calculations.

suggest that the oleic acid film is adhering onto all three of the crystalline cellulose planes. From the plot it can be observed that, once adhered (around 100 ps), the oleic acid molecules stay attached to the crystalline cellulose plane throughout the rest of the simulation. The degree of adhesion varied according to both the molecular surface roughness and amount of hydrogen bonding: the highest $W_{adhesion}$ was observed for the [010] plane that possesses the largest degree of molecular surface roughness and number of hydrogen bonding sites per area, followed by [110] and [100]. Interestingly, these results support the findings by Wågberg and co-workers,[27] who determined that the interdiffusion of oil vehicles of an ink into cellulose surfaces increased with an increase in molecular contact area due to the increased molecular surface roughness; subsequently, they observed an increase in the interfacial adhesion; dispersion and polar interaction forces were also suggested to play a significant role.

Therefore, the [010] plane with the largest molecular surface area as well as the greatest degree of molecular surface roughness and the number of accessible hydrogen bonding sites per area (Table 1) provides more attractive interactions for the oleic acid molecules. In contrast, the [110] and [100] planes with their relatively comparable surface areas and molecular surface roughness allow significant surface mobility of oleic acid molecules. Similar trends were observed as a function of surface roughness for the adsorption of the fibrinogen protein on crystalline tantalum surfaces using a combination of QCM measurements and Monte Carlo simulations.[70] Similarly, the adsorption of commonly used oils with polystyrene nanofibers were observed to increase with the increase in fiber surface area.[71] This understanding can be further exploited by incorporating cellulosic materials with increased surface area to capture oily substances.[72]

Based on the results from these MD simulations, we propose that surface roughness has a higher impact on the oleic acid adhesion on cellulose compared to the number of hydrogen bonds formed. This effect could be due to the location and accessibility of the hydrogen bonding sites available for each surface. Thus, surface roughness combined with hydrogen bonding is essential to understand oil buildup and organic contamination of cellulose surfaces. In comparison to an amorphous surface, with its lower density, more surface randomness, and overall increase in molecular surface roughness, there is a greater chance of surface penetration of the oleic acid molecules, and thus the MSD is expected to be much greater than is observed for the crystalline planes, and thus, the difference between the values obtained by three planes in Figure 5 is likely minimal. It can also be inferred that the adhered oleic acid film can hinder solvent accessibility to each underlying cellulose plane, which is crucial for detergency or contaminant removal as well as for applications where the surface needs to be cleaned.

In summary, molecular-scale features on the surface of cellulose affect the behavior when different crystal planes are exposed to organic molecules. Results from this study supports that crystalline cellulose surfaces can possess a strong degree of amphiphilicity, which increases with the degree of molecular surface roughness and subsequent availability of hydroxyl groups for hydrogen bonding. Previous papers by Mazeau and co-workers characterized the [100] and [110] planes as hydrophobic and hydrophilic, respectively, based on their contact angle values.[49] The [010] plane has been described as a hydrophilic plane with trenches.[73] Their results indicated that the number of hydrogen bonds is higher in [010] compared to [200], which is similar to the [100] plane. The potential energy results from their work indicated that the electrostatic energy has a dominant role in adsorption of hydrophobic lignin on both the [200] and [010] planes. They also indicated that the availability of the hydroxyl groups for hydrogen bonding is dictated by its structure. The [010] plane possesses a trench-line feature that allows the hydroxyl groups to protrude outward and can entrap the molecules within the structure. Both of these facts have been verified in our study where potential energy components of OA adsorption on cellulose was found to be dominated by electrostatics for all three planes. It was also determined that structural features allowed the [010] plane to adsorb more OA molecules compared to [100] due to its availability of hydroxyl groups within the plane grooves.

The highest adsorption of amphiphilic OA molecules on the most hydrophilic [010] cellulose plane supports its amphiphilic nature. This amphiphilic nature of cellulose lies in its chemical (presence of hydroxyl groups and their polarity) and physical (surface area, presence of narrow grooves) properties. This nature could be a reason why hydrophobic impurities adsorb onto the cell wall of the cellulosic structures as well as its insolubility in water.[32] The resultant attraction from the

dx.doi.org/10.1021/bm500088c | Biomacromolecules XXXX, XXX, XXX−XXX

nonbonding (vdW and electrostatic) interactions allows the oil film to stay attached on the surface, which might hinder its removal.

Such information enables better supported decisions and predictions of the performance of devices used to collect or passivate oil deposits in various products or processes. Based on the presented results, it is proposed that increasing the amount of molecular surface roughness and the number of available hydroxyl groups will lead to greater adhesion of polar fatty acid films on cellulose. Thus, the density of hydroxyl groups should be minimized in order to increase film formation, and maximized for oil cleanup purposes. Similar conclusions were drawn from experiments performed on, for example, biofilm formation on polymeric surfaces[74] and bacterial attachment on stainless steel surfaces.[75] Conversely, ink adhesion was recently observed to increase due to increased mobility of the ink molecules and increased contact area.[76] Knowledge of surface roughness, charges, and molecular characteristics is crucial for developing products with tunable adhesion, such as those with variable hydrophilicity and hydrophobicity.[77,78]

■ CONCLUSIONS

This study offered molecular details about the effects of surface chemistry and molecular surface roughness on the adhesion of an oleic acid film on crystalline cellulose planes using MD simulations. Oleic acid was observed to adhere on all three crystalline cellulose planes. The strength of adhesion was greatest on the [010] crystal plane due to its increased surface area, molecular roughness and the presence of higher density hydrogen bonding sites. The [100] and [110] planes had similar adhesion values, despite the presence of small molecular-scale grooves on the [110] plane, which seem to be too small to enable more hydrogen bonding sites and interpenetration of the OA molecules. The results of this work helps to understand how hydrogen bonding and molecular roughness impact the adhesion of fatty acids to crystalline cellulose surfaces, which could be adapted for many practical applications, such as reducing the amount of energy required to remove these oily deposits from cellulose surfaces or hindering biofilm growth.

■ AUTHOR INFORMATION

Corresponding Author

*E-mail: melissa_pasquinelli@ncsu.edu. Phone: (919) 515-9426.

Present Address

[†]Whirlpool Corporation, 750 Monte Road, MD-5155, Benton Harbor, MI 49022, United States.

Notes

The authors declare no competing financial interest.

■ ACKNOWLEDGMENTS

The authors would like to thank Whirlpool Corporation for funding this work through a graduate fellowship to M.A.A.R.Q.

■ REFERENCES

(1) Kallio, T.; Laine, J.; Stenius, P. Intermolecular interactions and the adhesion of oleic acid. *J. Dispersion Sci. Technol.* **2009**, *30*, 222−230.

(2) Johansson, I.; Somasundaran, P. *Handbook for Cleaning/Decontamination of Surfaces*; Elsevier: New York, 2007 (available online).

(3) Lundgren, S. M.; Persson, K.; Mueller, G.; Kronberg, B.; Clarke, J.; Chtaib, M.; Claesson, P. M. Unsaturated fatty acids in alkane solution: adsorption to steel surfaces. *Langmuir* **2007**, *23*, 10598−10602.

(4) Lee, H. J.; Michielsen, S. Preparation of a superhydrophobic rough surface. *J. Polym. Sci., Part B: Polym. Phys.* **2007**, *45*, 253−261.

(5) Wu, W.; Zhu, Q.; Qing, F.; Han, C. C. Water repellency on a fluorine-containing polyurethane surface: toward understanding the surface self-cleaning effect. *Langmuir* **2008**, *25*, 17−20.

(6) Bhushan, B.; Jung, Y. C.; Koch, K. Micro-, nano-and hierarchical structures for superhydrophobicity, self-cleaning and low adhesion. *Philos. Trans. R. Soc., A* **2009**, *367*, 1631−1672.

(7) Kim, S.; Cheung, E.; Sitti, M. Wet self-cleaning of biologically inspired elastomer mushroom shaped microfibrillar adhesives. *Langmuir* **2009**, *25*, 7196−7199.

(8) Fürstner, R.; Barthlott, W.; Neinhuis, C.; Walzel, P. Wetting and self-cleaning properties of artificial superhydrophobic surfaces. *Langmuir* **2005**, *21*, 956−961.

(9) Lee, J.; Fearing, R. S. Contact self-cleaning of synthetic gecko adhesive from polymer microfibers. *Langmuir* **2008**, *24*, 10587−10591.

(10) Hu, Z.; Zen, X.; Gong, J.; Deng, Y. Water resistance improvement of paper by superhydrophobic modification with microsized $CaCO_3$ and fatty acid coating. *Colloids Surf., A* **2009**, *351*, 65−70.

(11) Dankovich, T. A.; Hsieh, Y.-L. Surface modification of cellulose with plant triglycerides for hydrophobicity. *Cellulose* **2007**, *14*, 469−480.

(12) Amin, I. N. H. M.; Mohammad, A. W.; Markom, M.; Peng, L. C. Effects of palm oil-based fatty acids on fouling of ultrafiltration membranes during the clarification of glycerin-rich solution. *J. Food Eng.* **2010**, *101*, 264−272.

(13) Barbar, R.; Durand, A.; Ehrhardt, J.; Fanni, J.; Parmentier, M. Physicochemical characterization of a modified cellulose acetate membrane for the design of oil-in-water emulsion disruption devices. *J. Membr. Sci.* **2008**, *310*, 446−454.

(14) Xhanari, K.; Syverud, K.; Chinga-Carrasco, G.; Paso, K.; Stenius, P. Structure of nanofibrillated cellulose layers at the o/w interface. *J. Colloid Interface Sci.* **2011**, *356*, 58−62.

(15) Bilbao-Sáinz, C.; Avena-Bustillos, R. J.; Wood, D. F.; Williams, T. G.; McHugh, T. H. Composite edible films based on hydroxypropyl methylcellulose reinforced with microcrystalline cellulose nanoparticles. *J. Agric. Food Chem.* **2010**, *58*, 3753−3760.

(16) Nguyen, J.; Reul, R.; Betz, T.; Dayyoub, E.; Schmehl, T.; Gessler, T.; Bakowsky, U.; Seeger, W.; Kissel, T. Nanocomposites of lung surfactant and biodegradable cationic nanoparticles improve transfection efficiency to lung cells. *J. Controlled Release* **2009**, *140*, 47−54.

(17) Cho, C.-W.; Choi, J.-S.; Shin, S.-C. Development of the ambroxol gels for enhanced transdermal delivery. *Drug Dev. Ind. Pharm.* **2008**, *34*, 330−335.

(18) Martín Alfonso, J.; Yañez, R.; Valencia, C.; Franco, J.; Diaz, M. Optimization of the methylation conditions of Kraft cellulose pulp for its use as a thickener agent in biodegradable lubricating greases. *Ind. Eng. Chem. Res.* **2009**, *48*, 6765−6771.

(19) Ingram, M.; Spikes, H.; Noles, J.; Watts, R. Contact properties of a wet clutch friction material. *Tribol. Int.* **2010**, *43*, 815−821.

(20) Flemming, H.-C.; Wingender, J. The biofilm matrix. *Nat. Rev. Microbiol.* **2010**, *8*, 623−633.

(21) Gross, R. A.; Kalra, B. Biodegradable polymers for the environment. *Science* **2002**, *297*, 803−807.

(22) Quéré, D. Wetting and roughness. *Annu. Rev. Mater. Res.* **2008**, *38*, 71−99.

(23) Marmur, A. Solid-surface characterization by wetting. *Annu. Rev. Mater. Res.* **2009**, *39*, 473−489.

(24) Coddard, E. 7 Cleaner/Conditioner Systems: Surface Chemical Aspects. *Surfactants in Personal Care Products and Decorative Cosmetics*; CRC Press: Boca Raton, FL, 2010; p 137.

(25) Rahbar, M.; Ayatollahi, S.; Ghatee, M. The roles of nano-scale intermolecular forces on the film stability during wettability alteration

process of the oil reservoir rocks. Trinidad and Tobago Energy Resources Conference, 27−30 June 2010, Port of Spain, Trindad, SPE: worldwide, 2010.
(26) Weglinski, S.; Obendorf, S. K. Soil Distribution on Fabric After Laundering. *Text. Chem. Color.* **1985**, 17.
(27) Forsström, J.; Eriksson, M.; Wågberg, L. A new technique for evaluating ink−cellulose interactions: initial studies of the influence of surface energy and surface roughness. *J. Adhes. Sci. Technol.* **2005**, *19*, 783−798.
(28) Gardner, D. J.; Oporto, G. S.; Mills, R.; Samir, M. A. S. A. Adhesion and surface issues in cellulose and nanocellulose. *J. Adhes. Sci. Technol.* **2008**, *22*, 545−567.
(29) Suppakul, P.; Jutakorn, K.; Bangchokedee, Y. Efficacy of cellulose-based coating on enhancing the shelf life of fresh eggs. *J. Food Eng.* **2010**, *98*, 207−213.
(30) Rodionova, G.; Lenes, M.; Eriksen, Ø.; Gregersen, Ø. Surface chemical modification of microfibrillated cellulose: improvement of barrier properties for packaging applications. *Cellulose* **2011**, *18*, 127−134.
(31) Li, S.; Zhang, S.; Wang, X. Fabrication of superhydrophobic cellulose-based materials through a solution-immersion process. *Langmuir* **2008**, *24*, 5585−5590.
(32) Glasser, W. G.; Atalla, R. H.; Blackwell, J.; Brown, R. M., Jr; Burchard, W.; French, A. D.; Klemm, D. O.; Nishiyama, Y. About the structure of cellulose: debating the Lindman hypothesis. *Cellulose* **2012**, *19*, 589−598.
(33) Medronho, B.; Romano, A.; Miguel, M. G.; Stigsson, L.; Lindman, B. Rationalizing cellulose (in)solubility: reviewing basic physicochemical aspects and role of hydrophobic interactions. *Cellulose* **2012**, *19*, 581−587.
(34) Heiner, A. P.; Kuutti, L.; Teleman, O. Comparison of the interface between water and four surfaces of native crystalline cellulose by molecular dynamics simulations. *Carbohydr. Res.* **1998**, *306*, 205−220.
(35) Biermann, O.; Hädicke, E.; Koltzenburg, S.; Müller-Plathe, F. Hydrophilicity and lipophilicity of cellulose crystal surfaces. *Angew. Chem., Int. Ed.* **2001**, *40*, 3822−3825.
(36) Mazeau, K.; Vergelati, C. Atomistic modeling of the adsorption of benzophenone onto cellulosic surfaces. *Langmuir* **2002**, *18*, 1919−1927.
(37) Wang, L.; Zhang, Y.; Gao, P. A novel function for the cellulose binding module of cellobiohydrolase I. *Sci. China: Life Sci.* **2008**, *51*, 620−629.
(38) Helle, S. S.; Duff, S. J.; Cooper, D. G. Effect of surfactants on cellulose hydrolysis. *Biotechnol. Bioeng.* **1993**, *42*, 611−617.
(39) Proctor, A.; Adhikari, C.; Blyholder, G. Mode of oleic acid adsorption on rice hull ash cristobalite. *J. Am. Oil Chem. Soc.* **1995**, *72*, 331−335.
(40) Tharanathan, R. Biodegradable films and composite coatings: past, present and future. *Trends Food Sci. Technol.* **2003**, *14*, 71−78.
(41) Payne, K. C.; Jackson, C. D.; Aizpurua, C. E.; Rojas, O. J.; Hubbe, M. A. Oil spills abatement: factors affecting oil uptake by cellulosic fibers. *Environ. Sci. Technol.* **2012**, *46*, 7725−7730.
(42) *Materials Studio Software*, Version 5.5; Accelrys: San Diego, CA, 2010.
(43) Raffaini, G.; Ganazzoli, F. Molecular dynamics simulation of the adsorption of a fibronectin module on a graphite surface. *Langmuir* **2004**, *20*, 3371−3378.
(44) Montanari, L.; Frigerio, F. Spin-probe ESR and molecular modeling studies on calcium carbonate dispersions in overbased detergent additives. *J. Colloid Interface Sci.* **2010**, *348*, 452−459.
(45) Da Silva Perez, D.; Ruggiero, R.; Morais, L. C.; Machado, A. E.; Mazeau, K. Theoretical and experimental studies on the adsorption of aromatic compounds onto cellulose. *Langmuir* **2004**, *20*, 3151−3158.
(46) Mazeau, K. On the external morphology of native cellulose microfibrils. *Carbohydr. Polym.* **2011**, *84*, 524−532.
(47) Quddus, M. A. A. R.; Rojas, O. J.; Pasquinelli, M. A., Molecular dynamics simulations of the thermal stability of crystalline cellulose surfaces coated with oleic acid. In *Functional Materials from Renewable Sources*; American Chemical Society: Washington, DC, 2012; Vol. *1107*, pp 191−208.
(48) Azizi Samir, M. A. S.; Alloin, F.; Dufresne, A. Review of recent research into cellulosic whiskers, their properties and their application in nanocomposite field. *Biomacromolecules* **2005**, *6*, 612−626.
(49) Mazeau, K.; Rivet, A. Wetting the (110) and (100) surfaces of Iβ cellulose studied by molecular dynamics. *Biomacromolecules* **2008**, *9*, 1352−1354.
(50) Xie, X.-Q.; Chen, J.-Z. Data mining a small molecule drug screening representative subset from NIH PubChem. *J. Chem. Inf. Model.* **2008**, *48*, 465−475.
(51) Nishiyama, Y.; Langan, P.; Chanzy, H. Crystal structure and hydrogen-bonding system in cellulose Iβ from synchrotron X-ray and neutron fiber diffraction. *J. Am. Chem. Soc.* **2002**, *124*, 9074−9082.
(52) Fletcher, R.; Reeves, C. M. Function minimization by conjugate gradients. *Comput. J.* **1964**, *7*, 149−154.
(53) Hansen, C. M. *Hansen solubility parameters: a user's handbook*; CRC Press: Boca Raton, FL, 2007.
(54) Park, B.; Lorenz, C. D.; Chandross, M.; Stevens, M. J.; Grest, G. S.; Borodin, O. A. Frictional dynamics of fluorine-terminated alkanethiol self-assembled monolayers. *Langmuir* **2004**, *20*, 10007−10014.
(55) Gee, R. H.; Maiti, A.; Bastea, S.; Fried, L. E. Molecular dynamics investigation of adhesion between TATB surfaces and amorphous fluoropolymers. *Macromolecules* **2007**, *40*, 3422−3428.
(56) Tantishaiyakul, V.; Worakul, N.; Wongpoowarak, W. Prediction of solubility parameters using partial least square regression. *Int. J. Pharm.* **2006**, *325*, 8−14.
(57) Chauve, G.; Heux, L.; Arouini, R.; Mazeau, K. Cellulose poly(ethylene-*co*-vinyl acetate) nanocomposites studied by molecular modeling and mechanical spectroscopy. *Biomacromolecules* **2005**, *6*, 2025−2031.
(58) Yiapanis, G.; Henry, D. J.; Evans, E.; Yarovsky, I. Effect of surface composition and atomic roughness on interfacial adhesion between polyester and amorphous carbon. *J. Phys. Chem. C* **2007**, *111*, 3000−3009.
(59) Clancy, T.; Mattice, W. Computer simulation of polyolefin interfaces. *Comput. Theor. Polym. Sci.* **1999**, *9*, 261−270.
(60) Deng, M.; Tan, V.; Tay, T. Atomistic modeling: interfacial diffusion and adhesion of polycarbonate and silanes. *Polymer* **2004**, *45*, 6399−6407.
(61) Owens, D. Some thermodynamic aspects of polymer adhesion. *J. Appl. Polym. Sci.* **1970**, *14*, 1725−1730.
(62) Blake, T.; De Coninck, J. The influence of solid−liquid interactions on dynamic wetting. *Adv. Colloid Interface Sci.* **2002**, *96*, 21−36.
(63) Kisin, S.; Bozovic Vukic, J.; van der Varst, P. G. T.; de With, G.; Koning, C. E. Estimating the polymer-metal work of adhesion from molecular dynamics simulations. *Chem. Mater.* **2007**, *19*, 903−907.
(64) Mazeau, K.; Heux, L. Molecular dynamics simulations of bulk native crystalline and amorphous structures of cellulose. *J. Phys. Chem. B* **2003**, *107*, 2394−2403.
(65) Lowry, R. R.; Tinsley, I. J. Rapid colorimetric determination of free fatty acids. *J. Am. Oil Chem. Soc.* **1976**, *53*, 470−472.
(66) Bicerano, J. *Prediction of polymer properties*; CRC Press: Boca Raton, FL, 2002.
(67) Barton, A. F. *CRC handbook of solubility parameters and other cohesion parameters*; CRC Press: Boca Raton, FL, 1991.
(68) Cedeño, F. O.; Prieto, M. M.; Espina, A.; García, J. R. Measurements of temperature and melting heat of some pure fatty acids and their binary and ternary mixtures by differential scanning calorimetry. *Thermochim. Acta* **2001**, *369*, 39−50.
(69) Dirama, T. E.; Carri, G. A.; Sokolov, A. P. Role of hydrogen bonds in the fast dynamics of binary glasses of trehalose and glycerol: a molecular dynamics simulation study. *J. Chem. Phys.* **2005**, *122*, 114505.
(70) Rechendorff, K.; Hovgaard, M. B.; Foss, M.; Zhdanov, V.; Besenbacher, F. Enhancement of protein adsorption induced by surface roughness. *Langmuir* **2006**, *22*, 10885−10888.

(71) Wu, J.; Wang, N.; Wang, L.; Dong, H.; Zhao, Y.; Jiang, L. Electrospun porous structure fibrous film with high oil adsorption capacity. *ACS Appl. Mater. Interfaces* **2012**, *4*, 3207−3212.
(72) Hubbe, M. A.; Rojas, O. J.; Fingas, M.; Gupta, B. S. Cellulosic substrates for removal of pollutants from aqueous systems: a review. 3. Spilled oil and emulsified organic liquids. *BioResources* **2013**, 8.
(73) Besombes, S.; Mazeau, K. The cellulose/lignin assembly assessed by molecular modeling. Part 1: Adsorption of a threo guaiacyl β-O-4 dimer onto a Iβ cellulose whisker. *Plant Physiol. Biochem.* **2005**, *43*, 299−308.
(74) Jansen, B.; Kohnen, W. Prevention of biofilm formation by polymer modification. *J. Ind. Microbiol.* **1995**, *15*, 391−396.
(75) Rodriguez, A.; Autio, W. R.; McLandsborough, L. A. Effect of surface roughness and stainless steel finish on Listeria monocytogenes attachment and biofilm formation. *J. Food Prot.* **2008**, *71*, 170−175.
(76) Jiang, W.; Liu, H.; Ding, Y.; Tang, Y.; Shi, Y.; Yin, L.; Lu, B. Investigation of ink transfer in a roller-reversal imprint process. *J. Micromech. Microeng.* **2009**, *19*, 015033.
(77) Liu, M.; Jiang, L. Switchable adhesion on liquid/solid interfaces. *Adv. Funct. Mater.* **2010**, *20*, 3753−3764.
(78) Cox, J. D.; Curry, M. S.; Skirboll, S. K.; Gourley, P. L.; Sasaki, D. Y. Surface passivation of a microfluidic device to glial cell adhesion: a comparison of hydrophobic and hydrophilic SAM coatings. *Biomaterials* **2002**, *23*, 929−935.